Title

Spatial–temporal FUCCI imaging of each cell in a tumor demonstrates locational dependence of cell cycle dynamics and chemoresponsiveness

Journal

Cell Cycle, 13(13)

ISSN

1538-4101

Authors

Yano, Shuya
Zhang, Yong
Miwa, Shinji
et al.

Publication Date

2014-07-01

DOI

10.4161/cc.29156

Peer reviewed

Cell Cycle 13:13, 2110–2119; July 1, 2014; © 2014 Landes Bioscience

Spatial–temporal FUCCI imaging of each cell in a tumor demonstrates locational dependence of cell cycle dynamics and chemoresponsiveness

Shuya Yano[1,2,3], Yong Zhang[1], Shinji Miwa[1,2], Yasunori Tome[1,2], Yukihiko Hiroshima[1,2], Fuminari Uehara[1,2], Mako Yamamoto[1,2], Atsushi Suetsugu[1,2], Hiroyuki Kishimoto[3], Hiroshi Tazawa[4], Ming Zhao[1], Michael Bouvet[2], Toshiyoshi Fujiwara[3], and Robert M Hoffman[1,2,*]

[1]AntiCancer, Inc; San Diego, CA USA; [2]Department of Surgery; University of California, San Diego; La Jolla, CA USA; [3]Department of Gastroenterological Surgery; Okayama University Graduate School of Medicine, Dentistry, and Pharmaceutical Sciences; Okayama, Japan; [4]Center for Innovative Clinical Medicine; Okayama University Hospital; Okayama, Japan

Keywords: drug resistance, cell cycle, tumor, confocal laser microscopy, fluorescent proteins, FUCCI, tumor blood vessels, dormancy

Abbreviations: FUCCI, fluorescence ubiquitination cell cycle indicator; CLSM, confocal laser scanning microscopy; GFP, green fluorescent protein

The phase of the cell cycle can determine whether a cancer cell can respond to a given drug. We report here on the results of monitoring of real-time cell cycle dynamics of cancer cells throughout a live tumor intravitally using a fluorescence ubiquitination cell cycle indicator (FUCCI) before, during, and after chemotherapy. In nascent tumors in nude mice, approximately 30% of the cells in the center of the tumor are in G_0/G_1 and 70% in $S/G_2/M$. In contrast, approximately 90% of cancer cells in the center and 80% of total cells of an established tumor are in G_0/G_1 phase. Similarly, approximately 75% of cancer cells far from (>100 μm) tumor blood vessels of an established tumor are in G_0/G_1. Longitudinal real-time imaging demonstrated that cytotoxic agents killed only proliferating cancer cells at the surface and, in contrast, had little effect on quiescent cancer cells, which are the vast majority of an established tumor. Moreover, resistant quiescent cancer cells restarted cycling after the cessation of chemotherapy. Our results suggest why most drugs currently in clinical use, which target cancer cells in $S/G_2/M$, are mostly ineffective on solid tumors. The results also suggest that drugs that target quiescent cancer cells are urgently needed.

Introduction

Recently, Watson suggested that, in cancer cells, signals for growth and cell division are always switched on, in contrast to the alternating switching on and off in normal cells.[1] Watson said that novel drugs should target the mechanisms that keep cancer cells switched on to proliferate. However, although Watson's characterization may apply to cancer cells in a dish, it may not apply to cancer cells in a tumor. In a tumor, a cancer cell's position in the cell cycle may be affected by access to nutrients and oxygen and other factors such as cell density and proximity to particular stromal elements.[2-4] However, the cell cycle status of individual cells in real time in a solid tumor is not well understood.[5-8] Sakaue-Sawano et al. have reported that the cell cycle phase in viable cells can be visualized using the fluorescent ubiquitination-based cell cycle indicator (FUCCI) system.[9]

We recently demonstrated, using FUCCI imaging, real-time visualization of the cell cycle kinetics of invading cancer cells in 3-dimensional (3D) Gelfoam® histoculture, which is in vivo-like.[10] Cancer cells in G_0/G_1 phase in Gelfoam® histoculture migrated more rapidly and further than the cancer cells in $S/G_2/M$ phase. After entry into $S/G_2/M$ phases, cancer cells ceased migrating and restarted migrating after division when the cells re-entered G_0/G_1. Migrating cancer cells were resistant to cytotoxic chemotherapy, since they were mostly in G_0/G_1, where cytotoxic chemotherapy is not effective.

In the present report, using intravital FUCCI imaging, the real-time relationship between cancer cell location in a tumor, cell cycle phase, and drug response are demonstrated. Our results indicate why current cytotoxic chemotherapy of most solid tumors generally ultimately fails clinically.

*Correspondence to: Robert M Hoffman; Email: all@anticancer.com
Submitted: 03/06/2014; Revised: 05/06/2014; Accepted: 05/07/2014; Published Online: 05/08/2014
http://dx.doi.org/10.4161/cc.29156

Results

Longitudinal FUCCI intravital imaging of a tumor growing on the liver

The cell cycle dynamics of FUCCI-expressing MKN45 human gastric cancer cells in a tumor that was growing in the liver was determined. A skin-flap abdominal imaging window[11-13] was used to longitudinally visualize the cell cycle phase of cancer cells within tumors using FUCCI and confocal laser scanning microscopy (CLSM) (**Fig. 1A**). The reversible skin-flap window enabled us to repeatedly perform CLSM. In nascent tumors, 7 d after implantation, there were cancer cells with red (G_1/G_0) and green ($S/G_2/M$) nuclei (**Fig. 1B, E, and H**). A rapidly growing tumor that reached more than 5 mm diameter 90 d after implantation had approximately 80% red (G_1/G_0) nuclei and 20% green ($S/G_2/M$) nuclei (**Fig. 1C, F, and H**). In contrast, in slowly growing tumors, almost all cancer cells had red nuclei (greater than 95%) (**Fig. 1D, G, and H**).

The location of cancer cells in a tumor determines cell cycle phase

CLSM permitted visualization of FUCCI-expressing cancer cells in a live tumor in vivo to a depth of ~250 μm (**Fig. 2**). The cell cycle of cancer cells at the surface and deep areas in tumors growing in the liver were compared. Seven days after implantation of FUCCI-expressing MKN45 human gastric cancer cells in the liver, intra-vital CLSM showed that 84.0% of the cancer cells were in S phase or G_2/M (**Fig. 2A and D**). In larger tumors, 21 and 35 d after implantation, 71.5% of the cancer cells near the tumor surface (0~100 μm) were in S phase or G_2/M, but in deep areas (>100 μm) of the tumor, 84.0% of the cancer cells were in G_0/G_1 phase (**Fig. 2B–D**). Cross sections of FUCCI-expressing tumors in the liver showed similar results as CLSM vertical-scanning images (**Figs. S1 and 2**). At 120 d after implantation, the cell cycle phase distribution was similar to that at 35 d (**Figs. S3–5**). These results demonstrated the vast majority of cancer cells in an established tumor are quiescent and possibly dormant, and only those at the surface of the tumor are proliferative (**Table S1**).

Next, we investigated how cancer cells in different locations changed cell cycle phase during tumor growth (**Fig. 2E**). We compared nascent (1–2 mm), medium-sized (4–6 mm), and larger (>10 mm) tumors. CLSM imaging showed that a nascent tumor (7 d after inoculation) consisted of cells that were mostly (90%) in $S/G_2/M$, even in the center and on the surface (**Fig. 2F and I**). In contrast, medium-sized established tumors (21 and 35 d after inoculation) had regions of both G_2/M cells (30–65%) and G_1/G_0 cells (35–70%) (**Fig. 2G–I**). Furthermore, the center of large-sized tumors (90 d after implantation) consisted of cells that were mostly (90%) in G_1/G_0 (**Figs. S2 and 3**; **Table S2**). The surface of the tumor consisted of cells mostly (70~80%) in $S/G_2/M$ regardless of time after implantation and tumor size, indicating that the cancer cells near the tumor surface were frequently cycling.

Cancer cells near tumor blood vessels are cycling

To investigate the cell cycle positions of cancer cells near and far from vessels,[14] CLSM time-course imaging was performed on a FUCCI-expressing tumor growing in the liver of transgenic nude mice in which the nestin promoter drives GFP expression (nestin-driven GFP [ND-GFP])[15] and thereby labels nascent blood vessels with GFP.[16-18] The number of nascent blood vessels in small rapidly growing tumors was more than in slowly growing tumors (**Fig. 3A and B**). The larger growing tumors have more nascent tumor vessels than smaller tumors (**Fig. 3A and B**). Therefore, we investigated the relationship between cell cycle phase and nascent tumor blood vessels. For cells <100 μm from a vessel, the fraction of $S/G_2/M$ cells was 66%, and the fraction of G_0/G_1 cells was 34% (**Fig. 3C and D**; **Fig. S6**; **Table S3**). In contrast, for cells >100 μm from a vessel, the fraction of $S/G_2/M$ cells was 25%, and fraction of G_0/G_1 cells was 75% (**Fig. 3C and D**; **Fig. S6**, **Table S3**). Time-course intravital imaging demonstrated that quiescent G_0/G_1 cancer cells far from vessels remained in G_0/G_1. Additional cancer cells entered G_0/G_1 in the tumors grown for 28 d compared with the tumors at 14 d (**Fig. 3E**).

Visualization of efficacy of cytotoxic chemotherapy on individual cancer cells in different cell cycle phases within tumors

In order to demonstrate the role of the cancer cell cycle phase in tumor drug resistance,[17-20] we treated a FUCCI-expressing rapid-growing tumor with cisplatinum (CDDP) or paclitaxel (**Fig. 4A**). Before treatment, the tumor had 68% of cells in $S/G_2/M$ and 32% of cells in G_1/G_0. Seven days after the last treatment, the tumor consisted of cancer cells mostly in G_0/G_1 phase (more than 90%), both at the surface and in the center of the tumor. These results suggest that CDDP or paclitaxel killed only proliferating cancer cells and had little effect on quiescent cancer cells (**Fig. 4B–F**). Fourteen days after the last treatment, the tumor again had cancer cells in $S/G_2/M$ phases at the surface. These results suggested that quiescent cancer cells resistant to cytotoxic agents resumed cycling after treatment (**Fig. 4B–E**). By 21 d after the last treatment, FUCCI-expressing tumors were growing (**Fig. 4B–E**). Cell cycle dynamics and change of tumor size were imaged for more than 30 d (**Fig. 4**). Our in vivo imaging system with FUCCI demonstrated longitudinally that currently-used chemotherapy kills only proliferating cancer cells and quiescent cancer cells are resistant.

The efficacy of cytotoxic chemotherapy depends on cell cycle phase of cancer cells, not tumor size

Furthermore we investigated the relationship between the ratio of cancer cells in G_0/G_1 phase or tumor size and drug resistance.[21,22] First, we treated the nascent tumors that consisted of cancer cells mostly in $S/G_2/M$ phases with CDDP or paclitaxel. Chemotherapy killed most cancer cells in $S/G_2/M$ phases and shrank tumor size (**Fig. 5A, B, E, and F**). In contrast, when we treated slow-growing tumors that consisted of cancer cells mostly in G_0/G_1 phase with CDDP or paclitaxel, there was little effect on cell cycle phase and tumor size (**Fig. 5C–F**). The ratio of cancer cells in G_0/G_1 phase was closely associated with the response of tumors to chemotherapy (**Fig. 5F**). These data indicated that cell cycle phase distribution within the tumor before chemotherapy determines the efficacy of chemotherapy.

Discussion

In the present report, we intravitally imaged the dynamics of the cell cycle of individual cancer cell throughout a tumor, both

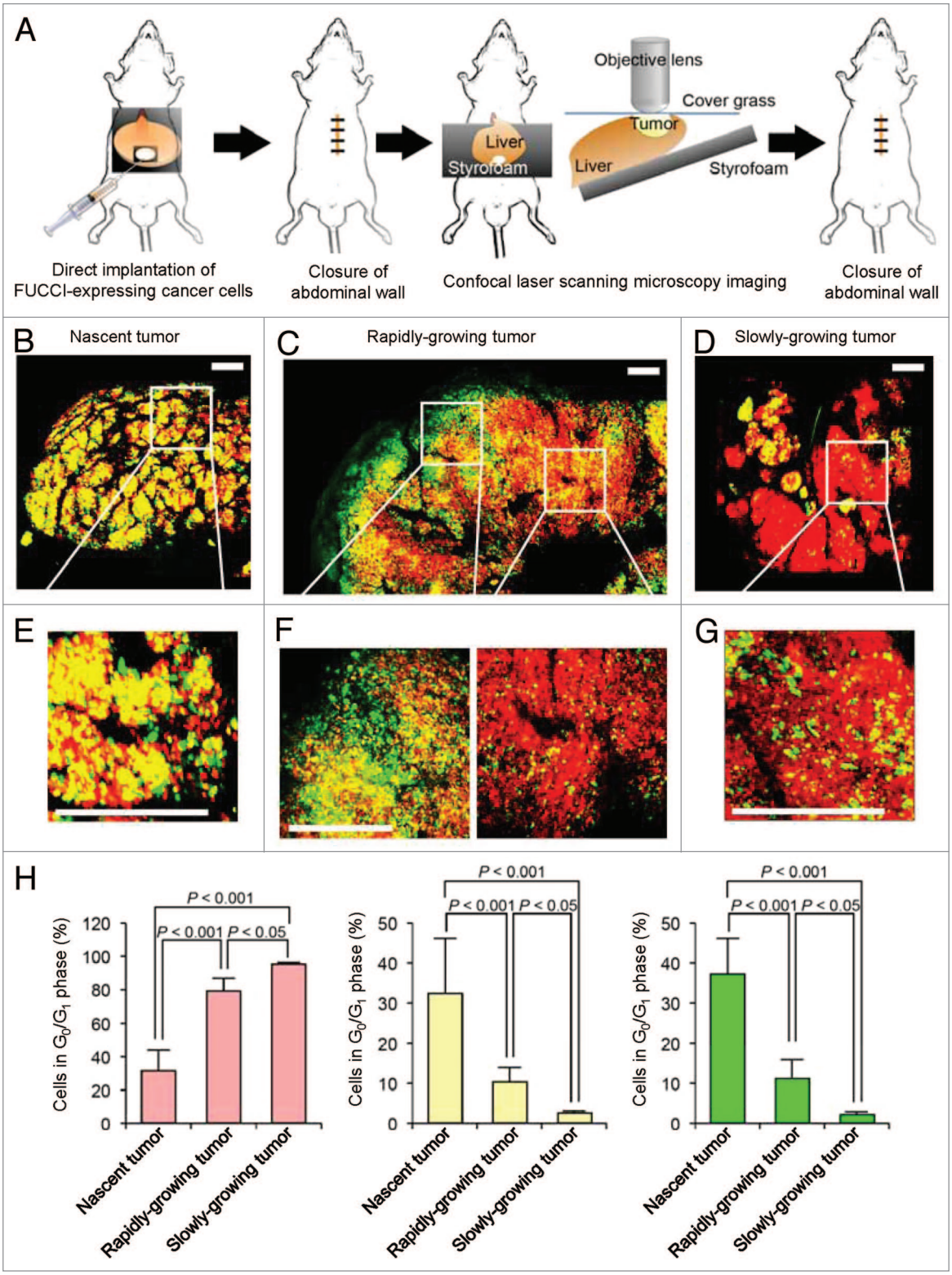

Figure 1. Intravital cell cycle imaging in FUCCI-expressing tumors growing in the liver. All images were acquired with the FV-1000 (Olympus) confocal laser scanning microscope (CLSM). The FUCCI-expressing cancer cells in G_0/G_1, S, or G_2/M phases appear red, yellow, or green, respectively. (**A**) Schematic diagram shows the method of repeated intravital CLSM imaging of FUCCI-expressing gastric-cancer cells growing in the liver. (**B–D**) Representative images of FUCCI-expressing tumors in the liver of live mice. Nascent tumor 7 d after implantation (**B**), rapidly growing tumor 90 d after implantation (**C**), slowly growing tumor 90 d after implantation (**D**). (**E–G**) High-magnification images of FUCCI-expressing cancer cells are shown. (**H**). Histograms show the distribution of FUCCI-expressing cells in a nascent tumor, a rapidly growing tumor, and a slowly growing tumor. Data are means ± SD (each group for n = 10). Scale bars represent 500 μm.

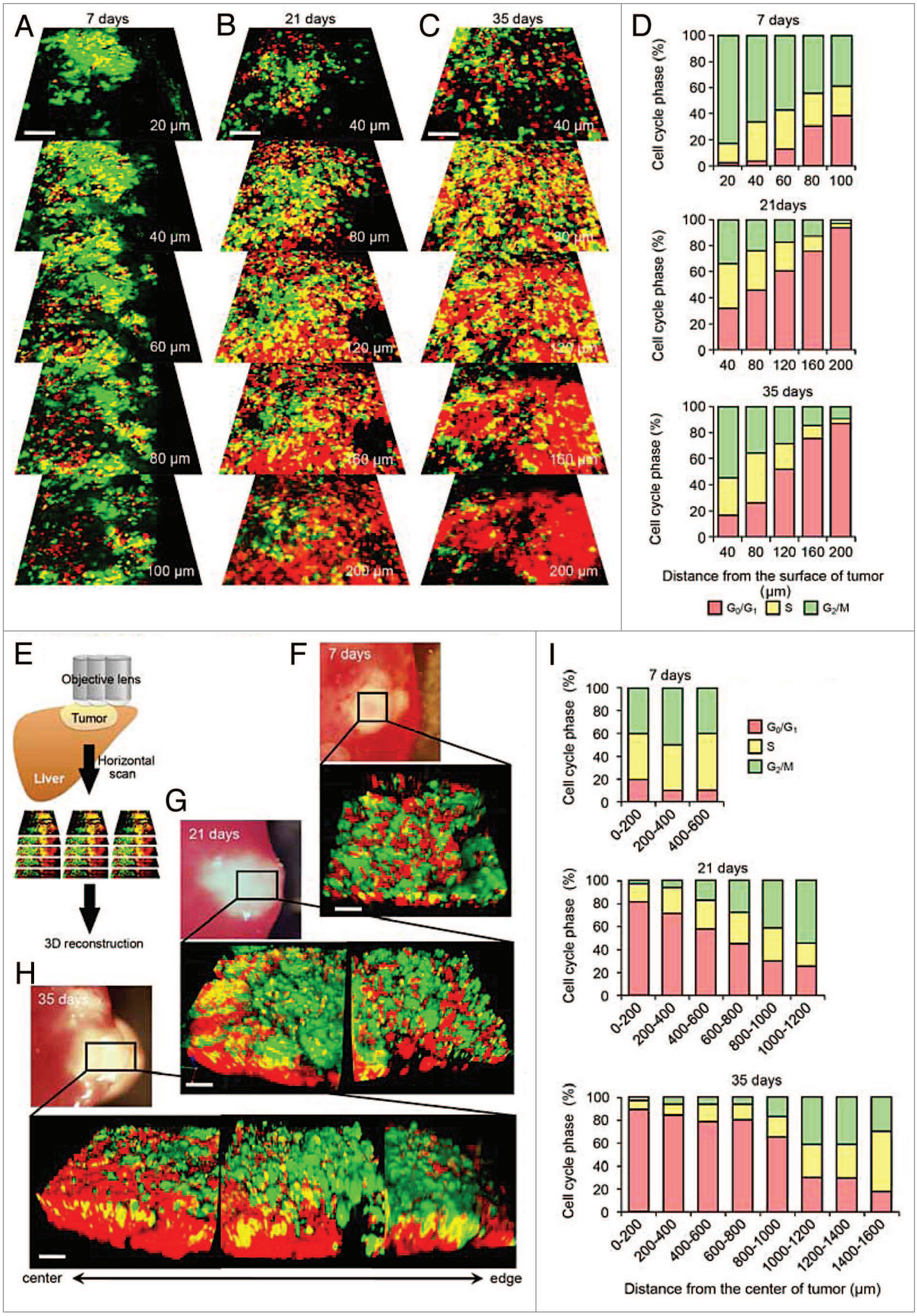

Figure 2. For figure legend, see page 2114.

Figure 2 (See previous page). Cell cycle phase distribution of cancer cells at the tumor surface and center. (**A–C**) FUCCI-expressing MKN45 cells were implanted directly in the liver of nude mice and imaged at 7 d (**A**), 21 d (**B**), or 35 d (**C**). (**D**) Histograms show the cell cycle distribution in the tumor at 7 d (top), 21 d (middle), and 35 d (lower) after implantation. (**E**) Schematic diagram of in vivo CLSM imaging of different sized tumors. Tumors were scanned from the center to the edge. The scanned images were then 3-dimensionally reconstructed. (**F–H**) Representative 3D reconstruction images of a nascent tumor at 7 d after cancer cell implantation (**F**), 21 d (**G**) and 35 d (**H**) after implantation. (**I**) Histogram shows the distribution of FUCCI-expressing cells at different distances from the center. The number of cells in each cell cycle phase were assessed by counting the number of cells of each color at the indicated time points and depth. The percentages of cells in the G_2/M, S, and G_0/G_1 phases of the cell cycle are shown (**E and I**). Data are means (each group for n = 5). Scale bars represent 100 μm.

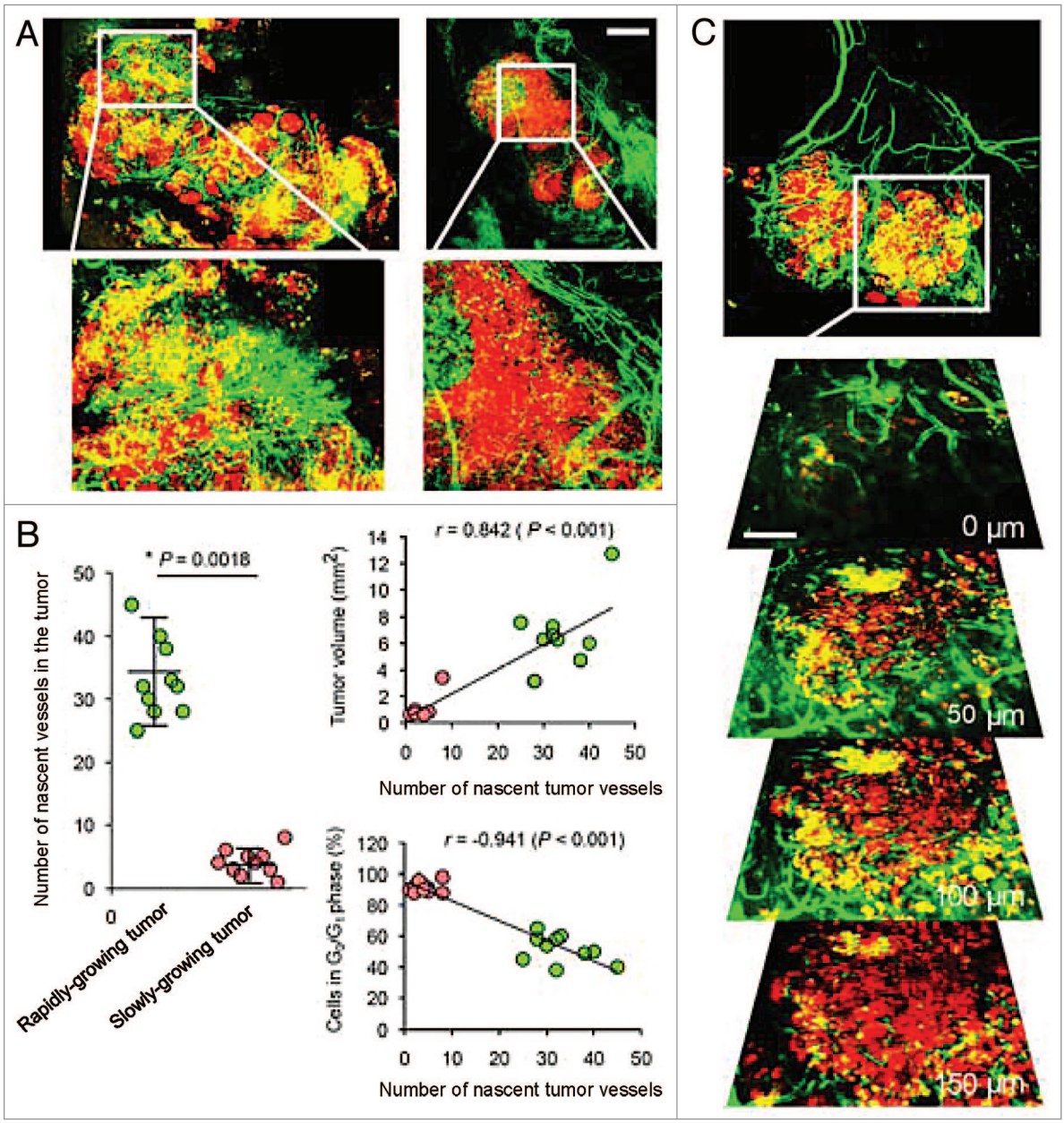

Figure 3A–C (See next page for panels D and E). Imaging nascent tumor vessels and cancer cell cycle phase in rapidly- and slowly-growing tumors. (**A**) Comparison of rapidly-growing tumors and slowly-growing tumors in ND–GFP transgenic mice, which labels nascent blood vessels with GFP. (**B**) Scatter-gram shows the number of GFP-expressing nascent tumor vessels in rapidly- and slowly-growing tumors (left). The number of nascent tumor vessels is associated with tumor volume (upper right). The number of nascent tumor vessels corresponds with the ratio of cancer cells in G_0/G_1 phase (lower right). (**C**) Images of FUCCI-expressing cancer cells in a large rapidly-growing tumor in the liver at 28 d after implantation are shown at different depths in the tumor. (**D**) Histogram shows the cell-cycle phase distribution at different distances (xy-plane) from blood vessels. Scale bars represent 100 μm. (**E**) Three-dimensional reconstruction of a tumor at 14 d (upper) and 28 d (lower) after implantation of FUCCI-expressing MKN45 cells in the liver of ND-GFP-expressing transgenic nude mice. Fine nascent blood vessels expressing GFP are indicated with arrowheads, and the trunk of blood vessels is indicated with arrows. Data are means (each group for n = 5). Scale bars represent (**A**) 500 μm; (**C**) 100 μm.

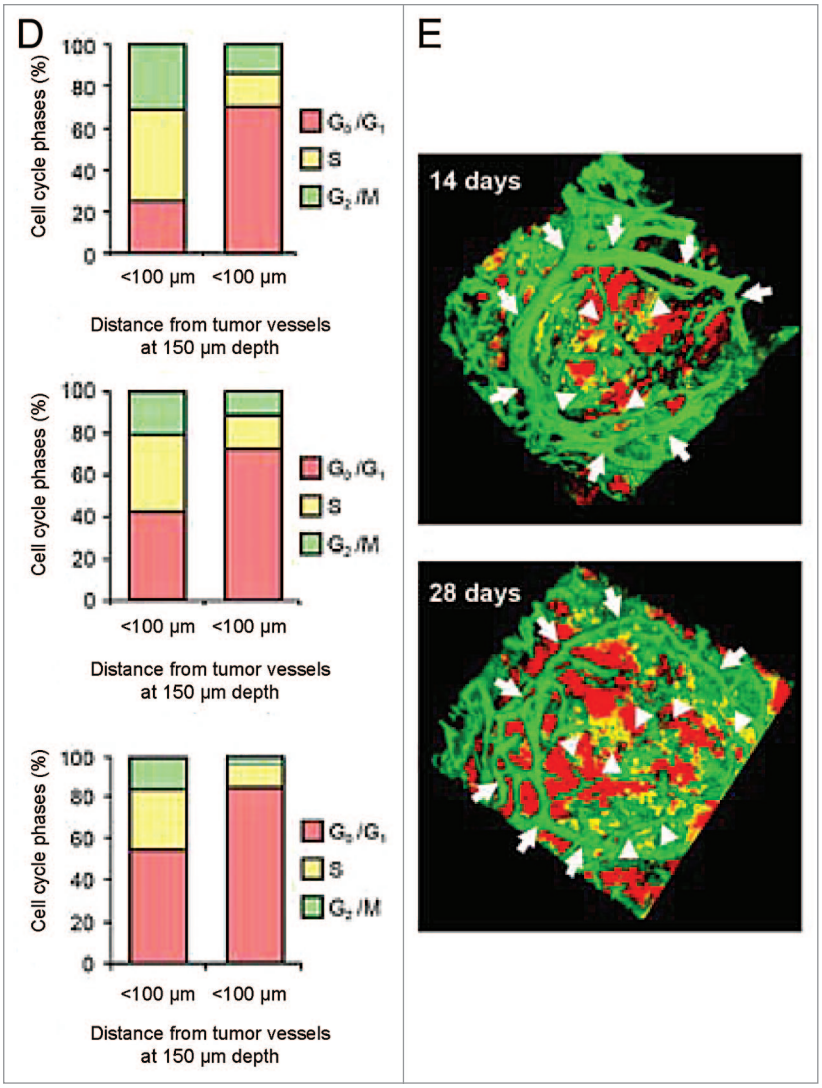

Figure 3D and E. For figure legend, see page 2114.

spatially and temporally and before and after chemotherapy. We visualized and characterized the cell-cycle dynamics of each cancer cell in tumors that were rapidly growing, slowly growing, and in nascent tumors and found a very different distribution of cell cycle phases among the cancer cells.[23,24] In the nascent tumors, a very large fraction (84.0%) of the cancer cells were in S/G_2/M phases. In contrast, in slow-growing tumors, which represent most metastatic solid tumors clinically, the vast majority of cancer cells was in G_0/G_1. We demonstrated that cytotoxic chemotherapy kills only cancer cells in S/G_2/M phases, which are in a minority in an established tumor, and had little effect on cancer cells in G_0/G_1 phase, which are the majority in an established tumor. Moreover, we showed the efficacy of chemotherapy depends not on tumor size, but the cell cycle phase of each cancer cell, which depends on the location in the tumor.

The results of this report indicate that most cancer cells in an established tumor are not always "switched on" to proliferate as Watson suggested.[1] It is just the opposite, most cancer cells in an established tumor are "switched off". We demonstrated that the vast majority of cancer cells in an established tumor are in G_0/G_1 phase and thereby resistant to cytotoxic chemotherapy. A solid tumor behaves very differently than cancer cells in a dish, where most cells can continually cycle. An established tumor contains quiescent cancer cells beneath the surface that are drug-resistant. Only the tumor surface and areas proximate to blood vessels had a majority of proliferating cancer cells.

We spatially and temporally demonstrated the cell cycle dynamics of individual cancer cells during tumor growth before, as well as during and after treatment with cytotoxic agents, within the same tumors. Our results explain why temporary regression may be often seen in the clinic after chemotherapy, as the drugs are effective only on cells in the outer layer of the tumor or near blood vessels, where cancer cells proliferate. Sakaue-Sawano et. al. captured an image of FUCCI-expressing subcutaneously growing HeLa cells, which mostly were cycling.[9] Our data showed that a mature tumor behaves very differently, with most cells quiescent, except at the tumor surface and near tumor blood vessels. Recurrence takes place when some of the quiescent cells re-enter the cell cycle as they replace the cycling cells killed by chemotherapy at the surface or near blood vessels.

Previously developed concepts and strategies of highly selective tumor targeting[26-37] can take advantage of spatial–temporal cell cycle imaging of a tumor described in the present report.

For example, the goal of tissue-selective therapy is to target normal and cancer cells of the same tissue, without toxicity to other tissues. Tissue-selective therapy focuses on unique properties of normal tissues and how therapy can target a property of a tissue that kills the cancer tissues that arise from the normal tissue without affecting other tissues. An example is anti-androgen therapy of prostate cancer. In order to improve cancer therapy, tissue-specific biochemical pathways must be identified and targeted, such as by prodrugs, in order to not cause toxicity to other normal tissue while eradicating the cancer. A subpopulation of a tissue can be targeted to reduce toxicity even further.[27,28]

Figure 4 (See opposite page). Spatial–temporal response to cytotoxic chemotherapy of cells in various phases of the cell cycle in tumors. (**A**) A schematic diagram showing longitudinal CSLM imaging of a FUCCI-expressing tumor after chemotherapy. (**B**) Representative image of a FUCCI-expressing tumor in the liver before and after CDDP treatment. (**C**) Images of FUCCI-expressing cancer cells are shown at different depths in the tumor at indicated time points. (**D**) Representative images of a FUCCI-expressing tumor in the liver before and after paclitaxel treatment. (**E**) Images of FUCCI-expressing cancer cells are shown at different depths in the tumor at indicated time points. (**F**) Histogram shows the cell-cycle phase distribution of cancer cells in the tumor at indicated time points. Data are means ± SD (each group for n = 5). Scale bars represent 500 μm.

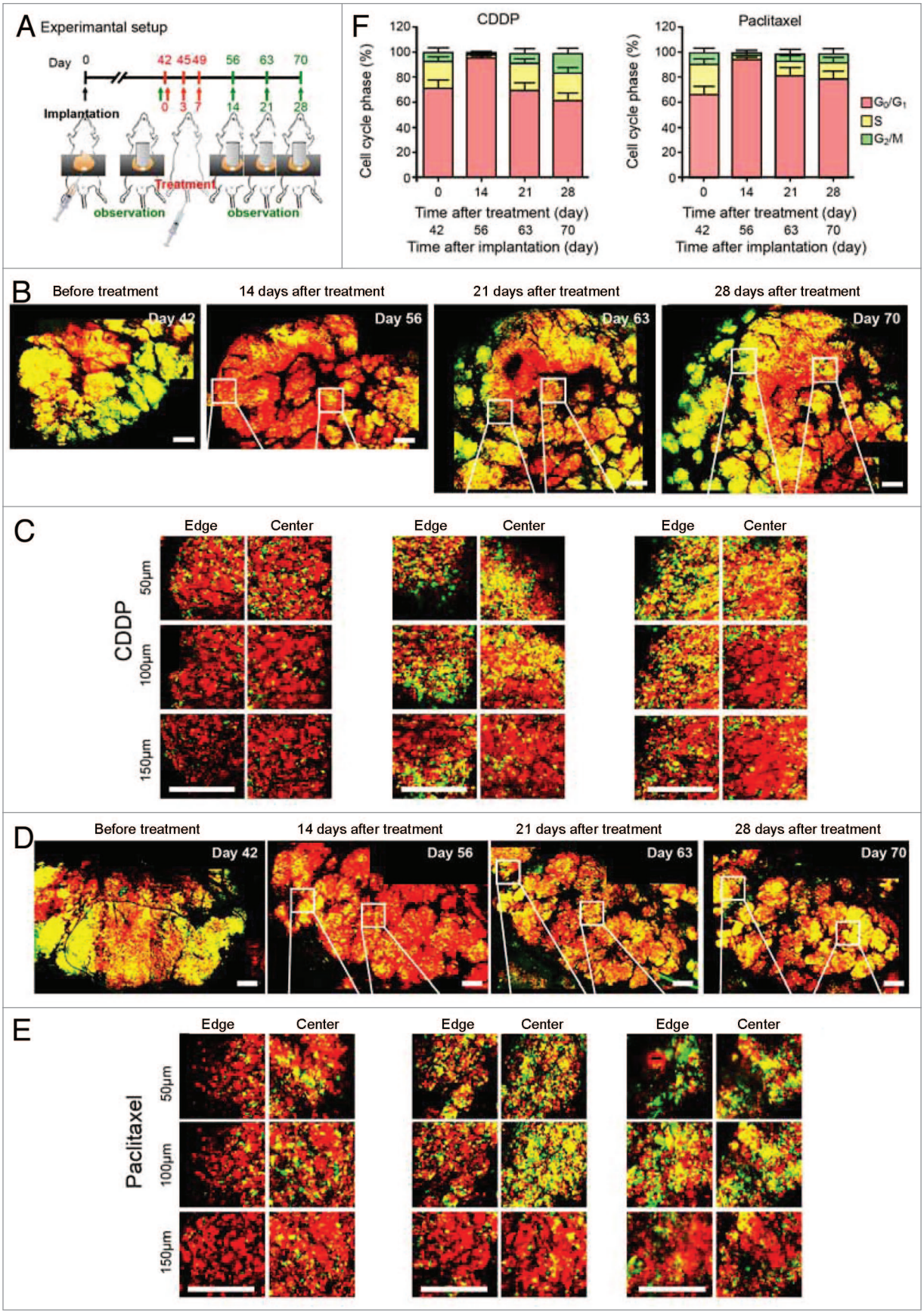

Figure 4. For figure legend, see page 2115.

De-differentiation of a tumor leading to therapy resistance is a limitation of tissue-selective therapy, since the targeted protein or pathway may no longer be expressed in the de-differentiated tumor. Therefore, tissue-selective therapy can be combined with differentiation therapy as well as anti-angiogenic and standard therapy for more effective outcomes or by novel approaches such as targeting of PSA, a prostate-specific protease, by prodrugs specifically cleaved by the protease in androgen-resistant prostate cancer.[27]

Certain caspases present in normal cells may not be expressed in drug-resistant cancer cells; therefore, specific caspase inhibitors could be used to selectively inhibit apoptosis in normal cells in the presence of pro-apoptotic drugs targeted to cancers in order to selectivity kill proliferating cancer cells.[28,31] For example in relapsed multidrug-resistant leukemia, treatment with caspase inhibitors to protect normal cells plus high doses of apoptosis-inducing chemotherapeutic drugs against drug-resistant leukemia cells, could induce remission without toxic side effects.[31]

Choriocarcinoma is highly aggressive, but very sensitive to cytotoxic chemotherapy that targets proliferating cells. Targeting rapidly proliferating cells in choriocarcinoma can result in cures. Choriocarcinoma may reactivate certain embryonic pathways, which may be targets of teratogens. Therefore, teratogens may be selectively toxic to choriocarcinoma or other embryonic cancers, whereas normal cells lack such pathways and should not be targeted by teratogens.[30]

It is necessary to kill proliferating cancer cells, in particular the dominant clones of proliferating cancer cells. In order to

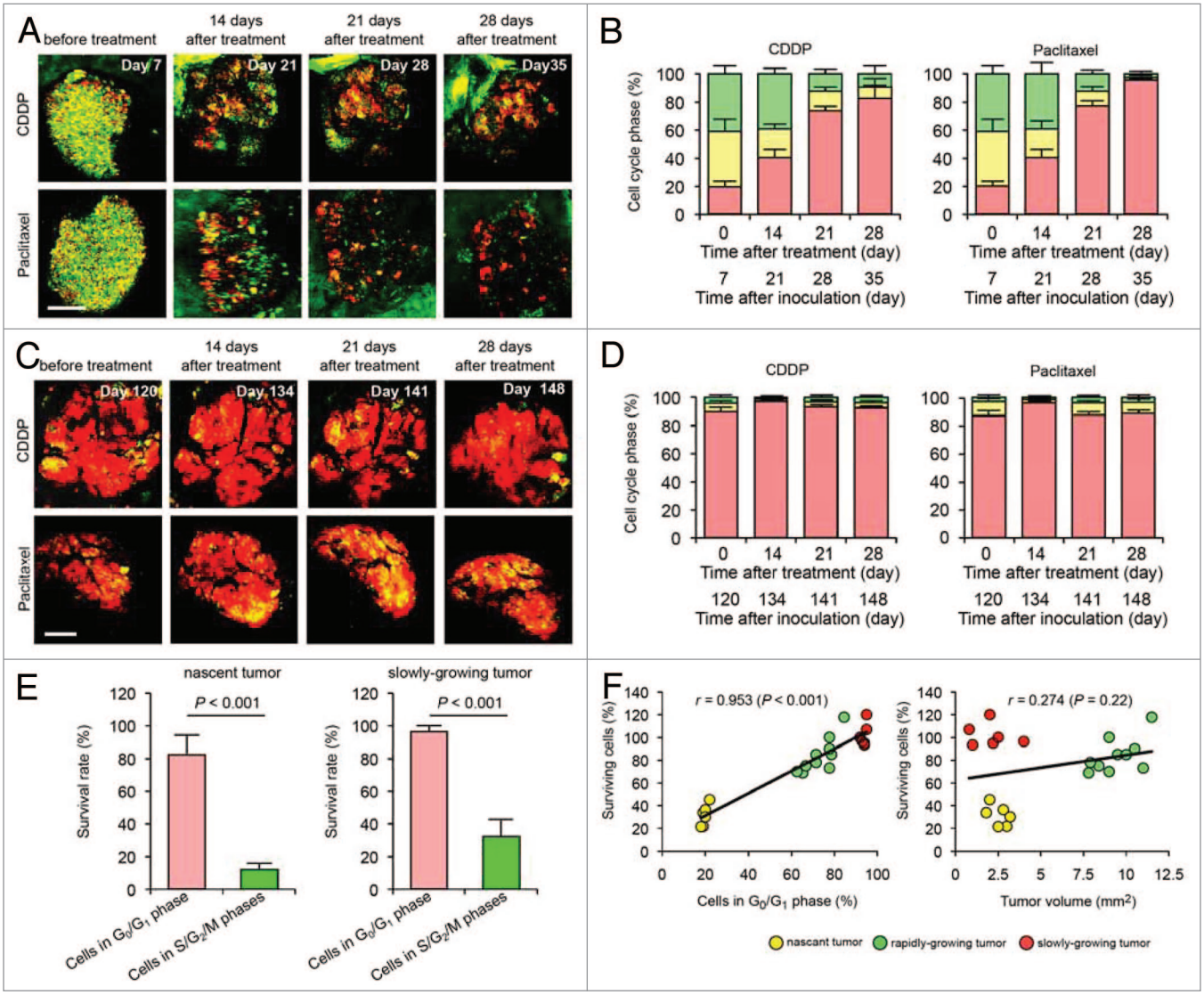

Figure 5. The efficacy of chemotherapy depends on the cell cycle phase distribution within the tumor. (**A**) Representative images of nascent FUCCI-expressing tumor in the liver before and after CDDP or paclitaxel treatment. (**B**) Histograms show the cell-cycle phase distribution within the tumor at the indicated time points. (**C**) Representative images of slowly growing FUCCI-expressing tumor in the liver before and after CDDP or paclitaxel treatment. (**D**) Histograms show the cell-cycle phase distribution within the tumor at the indicated time points. (**E**). Histograms show the survival rate of the cancer cells in G_0/G_1 phase or in $S/G_2/M$ phases after chemotherapy. (**F**) Relationship between the ratio of cells in G_0/G_1 phases before treatment and surviving cell fraction (left). Relationship between tumor size before treatment and surviving cell fraction (right). Data are means ± SD (each group for n = 3). Scale bars = 500 μm.

eradicate a cancer, it is possible to repeatedly target only proliferative cells.[37] Quiescent or dormant cells can resume proliferation; therefore, repeated cycles of therapy will be necessary to kill them once they resume proliferating. Cell cycle-dependent therapy can be combined with drugs that protect normal cells while eradicating even the most drug-resistant cancer cells.[32]

Normal cells can be protected from cell cycle-specific chemotherapeutic agents, including mitotic inhibitors such as paciltaxel. For example, rapamycin potentiates the protective effect of nutlin-3a, an inducer of wild-type p53 that causes G_1 or G_2 arrest in normal cells during paxlitaxel therapy, thereby protecting the normal cells from lethal mitotic arrest but not the cancer cells. In another approach, the combination of rapamycin and metformin induced G_1 and G_2 arrest selectively in normal cells and thereby protected them from the toxic mitotic-arrest effects of paclitaxel, which then acted only on mitotic cancer cells.[34]

Actinomycin D (LDActD) a p53 activator, was substituted for Nutlin-3 in p53-based cyclotherapy with an Aurora kinase inhibitor VX-680. LDActD protected normal fibroblasts from polyploidy induced by VX-680 by arresting them in G_1/G_0 and preventing them from entering S phase. It was proposed that drugs that are incorporated into DNA during S phase may have more selective efficacy against the cancer cells. S phase-dependent DNA-incorporating drugs can be used in combination during cyclotherapy with LDActD as a cytostatic agent for normal cells, which would then protect the normal cells from the S phase-dependent DNA-incorporating drugs that would only target cycling cancer cells.[35] Alternating treatment strategies can also be used, including tissue-specific oncotargeting, anti-proliferation with protection of normal cells, and differentiation therapy.

Spatial–temporal cell cycle imaging of tumors can yield valuable information to be used along with innovative strategies[26,27] to selectively target proliferating cells of the cancer as described above.

Early detection is very advantageous since smaller tumors have more proliferating cells, enabling the strategies outlined above to be even more effective.

The possibility of targeting resting cancer cells, while protecting normal cells, will be the topic of a future report.

Materials and Methods

Cells

MKN45 is a radio-resistant poorly-differentiated stomach adenocarcinoma-derived from a liver metastasis of a patient.[25] The cells were grown in RPMI 1640 medium with 10% fetal bovine serum and penicillin/streptomycin.

Establishment of MKN45 cells stably transfected with FUCCI-vector plasmids

For cell cycle-phase visualization, the FUCCI (fluorescent ubiquitination-based cell cycle indicator) expression system was used.[9] Plasmids expressing mKO2-hCdt1 (green fluorescent protein) or mAG-hGem (orange fluorescent protein) were obtained from the Medical and Biological Laboratory. Plasmids expressing mKO2-hCdt1 were transfected into MKN45 cells using Lipofectamine™ LTX (Invitrogen). The cells were incubated for 48 h after transfection and were then trypsinized and seeded in 96-well plates at a density of 10 cells/well. In the first step, cells were sorted into green (S, G_2, and M phase) cells using a FACSAria cell sorter (Becton Dickinson). The first-step-sorted green-fluorescent cells were then re-transfected with mAG-hGem (orange) and then sorted by orange fluorescence.

Animal experiments

Athymic *nu/nu* nude mice (AntiCancer, Inc) were maintained in a barrier facility under HEPA filtration and fed with autoclaved laboratory rodent diet (Teklad LM-485; Harlan). All animal studies were conducted in accordance with the principles and procedures outlined in the National Institute of Health Guide for the Care and Use of Animals under Assurance Number A3873-1.

Nestin-driven GFP (ND-GFP) transgenic nude mice

Nestin-driven green fluorescent protein (ND-GFP) transgenic C57/B6 mice carry the GFP gene under the control of the nestin promoter.[16-18] In the present study, the ND–GFP gene was crossed into nude mice on the C57/B6 background to obtain ND–GFP nude mice (AntiCancer Inc).[16-18]

Tumor model

All animal procedures were performed under anesthesia using s.c. administration of a ketamine mixture (10 μl ketamine HCl, 7.6 μl xylazine, 2.4 μl acepromazine maleate, and 10 μl PBS) (Henry-Schein). FUCCI-expressing MKN45 cells were harvested by brief trypsinization. Single-cell suspensions were prepared at a final concentration of 2×10^5 cells/5 μl Matrigel (Becton Dickinson). After laparotomy, the mouse liver was exteriorized and the cancer cells subserosally injected directly into the left lobe of the liver using a 31-gauge needle. After cancer cell implantation, the abdominal wall of mice was closed with 6–0 sutures.

Intravital confocal laser microscopy

The liver was exteriorized and a cover glass was gently put on the liver, which inhibited vibration caused by heartbeat and respiratory movement. Confocal laser scanning microscopy (CLSM) was performed using the FV-1000 (Olympus Corp) with 2-laser diodes (473 nm and 559 nm). A 4 × (0.20 numerical aperture immersion) objective lens and 20 × (0.95 numerical aperture immersion) objective lens (Olympus) were used. 800 × 800 pixels and 1.0-μm z steps were scanned, which took 1–2 s per section, with 6–8 min per full 3D scan. Scanning and image acquisition were controlled by Fluoview software (Olympus).

3D image analysis

The tracing data were imported to Volocity 6.0 version (Perkin Elmer), where all further analysis was performed.

Statistical analysis

Data are shown as means ± SD. For comparison between 2 groups, significant differences were determined using the Student's *t*-test.

Disclosure of Potential Conflicts of Interest

Y.Z. and M.Z. are employees of AntiCancer Inc. S.Y., S.M., Y.T., Y.H., F.U., M.Y., A.S., H.K. and R.M.H. are or were unsalaried associates of AntiCancer Inc. There are no other potential conflicts of interest disclosed.

Acknowledgments

We thank members of our laboratories for the critical reading of this manuscript and useful discussions. This work was supported in part by National Cancer Institute grant CA132971.

Authors Contributions

S.Y. and R.M.H. conceived the idea for this project. S.Y. and R.M.H. designed all experiments and wrote the manuscript. S.Y., Y.Z., S.M., Y.T., Y.H., F.U. and A.S. performed all experiments. M.Y., H.K., H.T., M.Z., M.B., and T.F. provided crucial ideas and helped with data interpretation. Y.Z. and H.T. provided special technical expertise.

Dedication

This paper is dedicated to the memory of A.R. Moossa, MD.

Supplemental Materials

Supplemental materials may be found here:
www.landesbioscience.com/journals/cc/article/29156

References

1. Watson JD. Curing "incurable" cancer. Cancer Discov 2011; 1:477-80; PMID:22586652; http://dx.doi.org/10.1158/2159-8290.CD-11-0220
2. Kyle AH, Baker JHE, Minchinton AI. Targeting quiescent tumor cells via oxygen and IGF-I supplementation. Cancer Res 2012; 72:801-9; PMID:22158947; http://dx.doi.org/10.1158/0008-5472.CAN-11-3059
3. Goss PE, Chambers AF. Does tumour dormancy offer a therapeutic target? Nat Rev Cancer 2010; 10:871-7; PMID:21048784; http://dx.doi.org/10.1038/nrc2933
4. Aguirre-Ghiso JA. Models, mechanisms and clinical evidence for cancer dormancy. Nat Rev Cancer 2007; 7:834-46; PMID:17957189; http://dx.doi.org/10.1038/nrc2256
5. Polzer B, Klein CA. Metastasis awakening: the challenges of targeting minimal residual cancer. Nat Med 2013; 19:274-5; PMID:23467237; http://dx.doi.org/10.1038/nm.3121
6. Marusyk A, Almendro V, Polyak K. Intra-tumour heterogeneity: a looking glass for cancer? Nat Rev Cancer 2012; 12:323-34; PMID:22513401; http://dx.doi.org/10.1038/nrc3261
7. Gottesman MM. Mechanisms of cancer drug resistance. Annu Rev Med 2002; 53:615-27; PMID:11818492; http://dx.doi.org/10.1146/annurev.med.53.082901.103929
8. Naumov GN, Townson JL, MacDonald IC, Wilson SM, Bramwell VH, Groom AC, Chambers AF. Ineffectiveness of doxorubicin treatment on solitary dormant mammary carcinoma cells or late-developing metastases. Breast Cancer Res Treat 2003; 82:199-206; PMID:14703067; http://dx.doi.org/10.1023/B:BREA.0000004377.12288.3c
9. Sakaue-Sawano A, Kurokawa H, Morimura T, Hanyu A, Hama H, Osawa H, Kashiwagi S, Fukami K, Miyata T, Miyoshi H, et al. Visualizing spatiotemporal dynamics of multicellular cell cycle progression. Cell 2008; 132:487-98; PMID:18267078; http://dx.doi.org/10.1016/j.cell.2007.12.033
10. Yano S, Miwa S, Mii S, Hiroshima Y, Uehara F, Yamamoto M, Kishimoto H, Tazawa H, Bouvet M, Fujiwara T, Hoffman RM. Invading cancer cells are predominantly in G0/G1 resulting in chemoresistance demonstrated by real-time FUCCI imaging. Cell Cycle 2014; 13:953-60; PMID:24552821; http://dx.doi.org/10.4161/cc.27818
11. Yamauchi K, Yang M, Jiang P, Xu M, Yamamoto N, Tsuchiya H, Tomita K, Moossa AR, Bouvet M, Hoffman RM. Development of real-time subcellular dynamic multicolor imaging of cancer-cell trafficking in live mice with a variable-magnification whole-mouse imaging system. Cancer Res 2006; 66:4208-14; PMID:16618743; http://dx.doi.org/10.1158/0008-5472.CAN-05-3927
12. Hoffman RM. The multiple uses of fluorescent proteins to visualize cancer in vivo. Nat Rev Cancer 2005; 5:796-806; PMID:16195751; http://dx.doi.org/10.1038/nrc1717
13. Condeelis J, Segall JE. Intravital imaging of cell movement in tumours. Nat Rev Cancer 2003; 3:921-30; PMID:14737122; http://dx.doi.org/10.1038/nrc1231
14. Jain RK. Normalization of tumor vasculature: an emerging concept in antiangiogenic therapy. Science 2005; 307:58-62; PMID:15637262; http://dx.doi.org/10.1126/science.1104819
15. Yang M, Baranov E, Wang JW, Jiang P, Wang X, Sun FX, Bouvet M, Moossa AR, Penman S, Hoffman RM. Direct external imaging of nascent cancer, tumor progression, angiogenesis, and metastasis on internal organs in the fluorescent orthotopic model. Proc Natl Acad Sci U S A 2002; 99:3824-9; PMID:11891294; http://dx.doi.org/10.1073/pnas.052029099
16. Li L, Mignone J, Yang M, Matic M, Penman S, Enikolopov G, Hoffman RM. Nestin expression in hair follicle sheath progenitor cells. Proc Natl Acad Sci U S A 2003; 100:9958-61; PMID:12904579; http://dx.doi.org/10.1073/pnas.1733025100
17. Amoh Y, Yang M, Li L, Reynoso J, Bouvet M, Moossa AR, Katsuoka K, Hoffman RM. Nestin-linked green fluorescent protein transgenic nude mouse for imaging human tumor angiogenesis. Cancer Res 2005; 65:5352-7; PMID:15958583; http://dx.doi.org/10.1158/0008-5472.CAN-05-0821
18. Mignone JL, Kukekov V, Chiang AS, Steindler D, Enikolopov G. Neural stem and progenitor cells in nestin-GFP transgenic mice. J Comp Neurol 2004; 469:311-24; PMID:14730584; http://dx.doi.org/10.1002/cne.10964
19. Junttila MR, de Sauvage FJ. Influence of tumour micro-environment heterogeneity on therapeutic response. Nature 2013; 501:346-54; PMID:24048067; http://dx.doi.org/10.1038/nature12626
20. Bock C, Lengauer T. Managing drug resistance in cancer: lessons from HIV therapy. Nat Rev Cancer 2012; 12:494-501; PMID:22673150; http://dx.doi.org/10.1038/nrc3297
21. Meads MB, Gatenby RA, Dalton WS. Environment-mediated drug resistance: a major contributor to minimal residual disease. Nat Rev Cancer 2009; 9:665-74; PMID:19693095; http://dx.doi.org/10.1038/nrc2714
22. Minchinton AI, Tannock IF. Drug penetration in solid tumours. Nat Rev Cancer 2006; 6:583-92; PMID:16862189; http://dx.doi.org/10.1038/nrc1893
23. Kreso A, O'Brien CA, van Galen P, Gan OI, Notta F, Brown AM, Ng K, Ma J, Wienholds E, Dunant C, et al. Variable clonal repopulation dynamics influence chemotherapy response in colorectal cancer. Science 2013; 339:543-8; PMID:23239622; http://dx.doi.org/10.1126/science.1227670
24. Giedt RJ, Koch PD, Weissleder R. Single cell analysis of drug distribution by intravital imaging. PLoS One 2013; 8:e60988; PMID:23593370; http://dx.doi.org/10.1371/journal.pone.0060988
25. Yokozaki H. Molecular characteristics of eight gastric cancer cell lines established in Japan. Pathol Int 2000; 50:767-77; PMID:11107048; http://dx.doi.org/10.1046/j.1440-1827.2000.01117.x
26. Blagosklonny MV. How cancer could be cured by 2015. Cell Cycle 2005; 4:269-78; PMID:15655345; http://dx.doi.org/10.4161/cc.4.2.1493
27. Blagosklonny MV. Tissue-selective therapy of cancer. Br J Cancer 2003; 89:1147-51; PMID:14520435; http://dx.doi.org/10.1038/sj.bjc.6601256
28. Blagosklonny MV. Matching targets for selective cancer therapy. Drug Discov Today 2003; 8:1104-7; PMID:14678733; http://dx.doi.org/10.1016/S1359-6446(03)02806-X
29. Blagosklonny MV. "Targeting the absence" and therapeutic engineering for cancer therapy. Cell Cycle 2008; 7:1307-12; PMID:18487952; http://dx.doi.org/10.4161/cc.7.10.6250
30. Blagosklonny MV. Teratogens as anti-cancer drugs. Cell Cycle 2005; 4:1518-21; PMID:16258270; http://dx.doi.org/10.4161/cc.4.11.2208
31. Blagosklonny MV. Treatment with inhibitors of caspases, that are substrates of drug transporters, selectively permits chemotherapy-induced apoptosis in multidrug-resistant cells but protects normal cells. Leukemia 2001; 15:936-41; PMID:11417480; http://dx.doi.org/10.1038/sj.leu.2402127
32. Blagosklonny MV. Target for cancer therapy: proliferating cells or stem cells. Leukemia 2006; 20:385-91; PMID:16357832; http://dx.doi.org/10.1038/sj.leu.2404075
33. Blagosklonny MV. Cancer stem cell and cancer stemloids: from biology to therapy. Cancer Biol Ther 2007; 6:1684-90; PMID:18344680; http://dx.doi.org/10.4161/cbt.6.11.5167
34. Apontes P, Leontieva OV, Demidenko ZN, Li F, Blagosklonny MV. Exploring long-term protection of normal human fibroblasts and epithelial cells from chemotherapy in cell culture. Oncotarget 2011; 2:222-33; PMID:21447859
35. Rao B, van Leeuwen IM, Higgins M, Campbel J, Thompson AM, Lane DP, Lain S. Evaluation of an Actinomycin D/VX-680 aurora kinase inhibitor combination in p53-based cyclotherapy. Oncotarget 2010; 1:639-50; PMID:21317459
36. Blagosklonny MV. NCI's provocative questions on cancer: some answers to ignite discussion. Oncotarget 2011; 2:1352-67; PMID:22267462
37. Blagosklonny MV. Antagonistic drug combinations that select against drug resistance: from bacteria to cancer. Cancer Biol Ther 2007; 6:1013-4; PMID:17646740; http://dx.doi.org/10.4161/cbt.6.7.4340